# Downregulating FGGY carbohydrate kinase domain containing promotes cell senescence by activating the p53/p21 signaling pathway in colorectal cancer

LIYA LIU[1-3*], MEIZHU WU[1,2*], YOUQIN CHEN[4*], YING CHENG[1,2], SIJIA LIU[1,2], XINRAN ZHANG[1,2], QIURONG XIE[1,2,5], LIUJING CAO[1,2], LIHUI WEI[1,2,5], YI FANG[1,2,5], ANJUM JAFRI[6], THOMAS J. SFERRA[4], ALING SHEN[1,2,5] and LI LI[7,8]

[1]Academy of Integrative Medicine, Fujian University of Traditional Chinese Medicine, Fuzhou, Fujian 350122, P.R. China; [2]Fujian Key Laboratory of Integrative Medicine on Geriatrics, Fujian University of Traditional Chinese Medicine, Fuzhou, Fujian 350122, P.R. China; [3]Department of Scientific Research, Affiliated Sanming Integrated Medicine Hospital of Fujian University of Traditional Chinese Medicine, Sanming, Fujian 365001, P.R. China; [4]Department of Pediatrics, Case Western Reserve University School of Medicine, Rainbow Babies and Children's Hospital, Cleveland, OH 44106, USA; [5]Innovation and Transformation Center, Fujian University of Traditional Chinese Medicine, Fuzhou, Fujian 350122, P.R. China; [6]Department of Genetics and Genome Sciences, Histology Core, Case Western Reserve University, Cleveland, OH 44106, USA; [7]Shengli Clinical College, Fujian Medical University, Fuzhou, Fujian 350001, P.R. China; [8]Department of Health Management, Fujian Provincial Hospital, Fuzhou University Affiliated Provincial Hospital, Fuzhou, Fujian 350001, P.R. China

Received July 4, 2024; Accepted January 14, 2025

DOI: 10.3892/ijmm.2025.5522

**Abstract.** Carbohydrate kinases serve an oncogenic role in several types of cancer; however, the function of FGGY carbohydrate kinase domain containing (FGGY) in colorectal cancer (CRC) remains unknown. The present study investigated the function and possible molecular mechanisms of FGGY in CRC. The results showed that elevated levels of FGGY mRNA and protein were observed in CRC tissues, and a higher expression of FGGY was associated with advanced N stage and reduced overall survival time in patients with CRC. Silencing FGGY inhibited the viability of CRC cells by inducing cell cycle arrest and promoting apoptosis *in vitro*, thereby attenuating tumor growth in a xenograft mouse model. FGGY knockdown also enriched the senescence-associated heterochromatin foci (SAHF) pathway and p53 pathway, as further confirmed by enhancing senescence-associated β-galactosidase (SA-β-gal) activity, with increased levels of SAHF-associated proteins HP1γ and trimethylation of H3K9 (H3k9me3) in CRC cells, as well as upregulation of p53 and its downstream protein p21. Furthermore, p53 knockout rescued FGGY knockdown-mediated reductions in cell viability, SA-β-gal activity, and the levels of HP1γ and H3k9me3 in CRC cells. These findings indicated that FGGY could act as a newly identified potential oncogene in CRC, partially through regulating the p53/p21 signaling pathway and altering cell senescence.

*Correspondence to:* Dr Aling Shen, Academy of Integrative Medicine, Fujian University of Traditional Chinese Medicine, 1 Qiuyang Road, Minhou, Fuzhou, Fujian 350122, P.R. China
E-mail: saling86@hotmail.com

Dr Li Li, Shengli Clinical College, Fujian Medical University, 134 East Street, Fuzhou, Fujian 350001, P.R. China
E-mail: lilifuzhou@126.com

*Contributed equally

*Key words:* olorectal cancer, FGGY, growth, senescence, p53 pathway

## Introduction

In 2020, it was estimated that >1.9 million new cases of colorectal cancer (CRC) were diagnosed globally, which was associated with ~935,000 deaths; this accounted for ~10% of all cancer incidences and deaths worldwide (1). Despite significant advances in diagnosis and treatment, CRC continues to have a high mortality rate and is a significant health burden worldwide (2-4). Therefore, conducting comprehensive research into the molecular mechanisms involved in the occurrence and development of CRC to identify potential molecular targets has scientific and clinical importance. This research could improve early diagnosis, prognostic assessment and the development of targeted treatments for CRC.

Our previous study conducted a screening for differentially expressed genes across 14 pairs of primary CRC lesions and adjacent non-cancerous tissues [Gene Expression Omnibus (GEO) accession no. GSE113513; https://www.ncbi.nlm.nih.gov/gds//] (5). This previous study revealed that the levels of FGGY carbohydrate kinase domain containing (FGGY) were elevated in CRC tissues (5). However, the functions

and biological mechanisms of FGGY in the progression of CRC are still largely unexplored. This motivated a further investigation into understanding the function of FGGY in CRC.

The FGGY gene is a member of the carbohydrate kinases family, which is evolutionarily conserved and known for its ability to phosphorylate an array of sugar substrates (6). The family of FGGY carbohydrate kinases includes enzymes such as L-fuculokinase, gluconokinase, glycerol kinase, D-ribulose kinase and L-xylulose kinase (7). FGGY was initially identified as being associated with sporadic amyotrophic lateral sclerosis (8,9). Moreover, FGGY has been reported to influence dietary obesity in mice by modulating lipid metabolism (9,10). In addition, a previous study revealed that functional variations in the FGGY gene are associated with the development and progression of lung squamous cell carcinoma (LUSC) (11). Notably, a tumor-specific and frequent L1-gene chimeric transcript involving FGGY (L1-FGGY) has been identified in LUSC. FGGY has been demonstrated to regulate cell proliferation and metabolic pathways (11,12). Nevertheless, its clinical significance and molecular mechanisms in CRC remain largely unexplored. The present study utilized gene expression datasets (GSE113513 and GSE20916) from the GEO, online bioinformatics databases, cDNA array-based quantification and a tissue microarray (TMA) to analyze FGGY expression in CRC samples. Furthermore, a series of *in vitro* and *in vivo* experiments were conducted with CRC cell lines and a nude mouse xenograft model to investigate the function and potential molecular mechanisms of FGGY in CRC.

## Materials and methods

*Bioinformatics analysis*. Differential gene expression analysis between cancer tissues and adjacent normal tissues was performed using The Cancer Genome Atlas (TCGA; https://cancergenome.nih.gov/) database and Gene Expression Profiling Interactive Analysis (GEPIA; http://gepia.cancer-pku.cn/) database. In the present study, the mRNA expression data of FGGY in both CRC and matched non-cancerous tissues were extracted from the GEO datasets (GSE20916 and GSE113513) (5,13) and TCGA (TCGA-COAD datasets) databases (14). Pearson correlation analysis was performed to evaluate the correlation between FGGY and p53 expression at the mRNA level in CRC using the GSE39582 GEO dataset (15) and TCGA-COAD datasets. Furthermore, the mRNA expression levels of FGGY in different types of digestive system cancer compared with in tissues from healthy controls were assessed using GEPIA (COAD datasets) (16).

*Cell lines and cell culture*. The CRC cell lines, HCT-8 (cat. no. TCHu18), Caco2 (cat. no. TCHu146), SW480 (cat. no. TCHu172), HCT116 (cat. no. TCHu99) and RKO (cat. no. TCHu116), and the colorectal adenocarcinoma cell line HT-29 (cat. no. TCHu103) were obtained from the National Collection of Authenticated Cell Cultures. The wild-type HCT116 cell line (HCT116/p53$^{+/+}$) and p53-knockout HCT116 cell line (HCT116/p53$^{-/-}$) were provided by Dr Yao Lin (Fujian University of Traditional Chinese Medicine, Fuzhou, China), which were originally sourced from Dr. Bert Vogelstein (Johns Hopkins University, Baltimore, MD, USA). HT-29 cells were cultured in McCoy's 5A medium (Nanjing KeyGen Biotech Co., Ltd.), whereas RKO cells were grown in MEM-α medium (Thermo Fisher Scientific, Inc.), Caco2 cells were maintained in DMEM (Thermo Fisher Scientific, Inc.), and HCT-8, HCT116, HCT116/p53$^{+/+}$ and HCT116/p53$^{-/-}$ cells were all maintained in RPMI1640 medium (Thermo Fisher Scientific, Inc.). Each cell line was incubated at 37˚C in a humidified atmosphere containing 5% $CO_2$. The growth media for all cells were supplemented with 10% FBS (Thermo Fisher Scientific, Inc.), 100 U/ml penicillin and 100 $\mu$g/ml streptomycin (Hyclone; Cytiva). The HT-29 cell line was characterized by Suzhou Jianda Biotechnology Co., Ltd. using short tandem repeat profiling.

*Reverse transcription-quantitative PCR (RT-qPCR)*. The total RNA was extracted from the cultured cells using RNAiso Plus reagent (Takara Biotechnology Co., Ltd.). RT into cDNA was performed using the PrimeScript RT reagent kit (Takara Biotechnology Co., Ltd.), strictly adhering to the guidelines provided by the manufacturer. In addition, a cDNA array of tissue samples, including 79 primary CRC and 15 adjacent noncancerous tissues (cat. no. HColA095Su01), was purchased from Shanghai Outdo Biotech Co., Ltd. The mRNA expression levels of FGGY and GAPDH were quantified using an ABI 7500 Fast Real-Time PCR System (Applied Biosystems; Thermo Fisher Scientific, Inc.) with SYBR Premix Ex Tag (Takara Biotechnology Co., Ltd.). The qPCR protocol consisted of an initial denaturation at 95˚C for 10 min, followed by 40 cycles of denaturation at 95˚C for 15 sec and annealing/extension at 60˚C for 60 sec. GAPDH was used as the internal control. The primer sequences are listed in Table SI. The mRNA expression levels were determined using the following formula: The relative expression levels were calculated using the $2^{-\Delta\Delta Cq}$ method, where $\Delta\Delta Cq$=[Cq(target gene)-Cq(GAPDH)]sample-[Cq(target gene)-Cq(GAPDH)]control (17). The experimental procedures and protocols of this research were approved by the Human Ethics Committee of Shanghai Outdo Biotech Co., Ltd. (no. SHYJS-CP-1704010). The clinicopathological characteristics of the patients with CRC included in the cDNA array are presented in Table SII.

*Immunohistochemistry (IHC) analysis of a TMA*. A TMA of CRC samples (including 101 CRC tissues and 79 adjacent noncancerous tissues; cat. no. HColA180Su15) and digestive system neoplasms [including colon adenocarcinoma (COAD), rectal adenocarcinoma (READ), pancreatic cancer (PAAD), esophageal cancer (ESCA), gastric cancer (STAD) and liver hepatocellular carcinoma (LIHC); including tumor tissues (COAD: 16; READ: 14; PAAD: 15; ESCA: 14; STAD: 14; LIHC: 16), normal tissues from healthy controls (colorectal tissues: 9; rectal tissues: 3; pancreatic tissues: 3; esophageal tissues: 5; gastric tissues: 7; liver tissues: 3) and adjacent noncancerous tissues (colorectal tissues: 16; rectal tissues: 14; pancreatic tissue: 15; esophageal tissues: 14; gastric tissues: 14; liver tissues: 16); cat. nos. HDgsC140PT01 and HorgC120PG04] were obtained from Shanghai Outdo Biotech Co., Ltd. IHC was performed to evaluate FGGY expression in clinical tumor samples, following previously described methods (5). Formalin-fixed, paraffin-embedded TMA

sections were dehydrated using graded ethanol and antigen retrieval was performed by microwave heating the slides for 20 min in sodium citrate-hydrochloric acid buffer (Fuzhou Maixin Biotechnology Development Co., Ltd.). After permeabilization with 0.1% Triton X-100 (cat. no. T8200; Beijing Solarbio Science & Technology Co., Ltd.) for 10 min, the sections were then treated with 3% $H_2O_2$ for 10 min at room temperature, followed by incubation with a blocking reagent (cat. no. KIT-9710; Fuzhou Maixin Biotechnology Development Co., Ltd.) for 30 min at room temperature. Tissue sections were then incubated with an antibody against FGGY (1:900; cat. no. PA5-120316; Thermo Fisher Scientific, Inc.) overnight at 4˚C, and with a secondary antibody (cat. no. KIT-9710; Fuzhou Maixin Biotechnology Development Co., Ltd.) for 1 h at room temperature. Immunoreactivity was then visualized using an enhanced DAB kit (cat. no. DAB-2031; Fuzhou Maixin Biotechnology Development Co., Ltd.). Images were captured using a Nano Zoomer 2.0 HT light microscope slide scanner (Hamamatsu Photonics K.K.) and processed using Nano Zoomer Digital Pathology View 1.6 software (Hamamatsu Photonics K.K.). To assess FGGY expression, a grading system was used; staining intensity was rated as follows: No staining, 0; weak, 1; moderate, 2; strong, 3; and the proportion of cells showing positive staining was rated as: 1-25%, 1; 26-50%, 2; 51-75%, 3; 76-100%, 4. The overall score for FGGY expression was determined by multiplying the intensity score with the percentage score.

For survival analysis, FGGY expression in CRC tissues was categorized into either low (final score, 0-6) or high (final score, 7-12). Kaplan-Meier survival curves were plotted for groups with high and low FGGY expression, and were analyzed using log-rank test. The experimental procedures and protocols of this research were approved by the Human Ethics Committee of Shanghai Outdo Biotech Co., Ltd. [nos. SHYJS-CP-1810005 (HColA180Su15), SHYJS-CP-1904003 (HDgsC140PT01), SHYJS-CP-1901007 (HorgC120PG04)]. The clinicopathological characteristics of patients with CRC are presented in Table SIII.

*Lentivirus transduction*. The specific short hairpin RNA (shRNA) targeting FGGY and a non-silencing control shRNA were designed and validated by Shanghai GeneChem Co., Ltd. The shRNA oligonucleotides were cloned into a GV248 lentiviral vector (Shanghai GeneChem Co., Ltd.) that included a green fluorescence protein (GFP) reporter gene. Briefly, a second-generation system was used and 293T cells were used as the interim cell line. For plasmid transfection, 293T cells were subcultured and seeded into 10-cm plates at a density of $5x10^6$ cells/15 ml. The DMEM was replaced with serum-free medium 2 h before transfection. A DNA solution containing 20 $\mu$g GV248 vector plasmid, 15 $\mu$g pHelper 1.0 carrier plasmid, 10 $\mu$g pHelper 2.0 vector plasmid and the corresponding volume of transfection reagent (cat. no. GRCT105; Shanghai GeneChem Co., Ltd.) was evenly mixed. The total volume was adjusted to 1 ml and incubated at room temperature for 15 min, then added dropwise to the 293T cells. After 6 h of transfection, the medium was replaced and 10 ml PBS was added. Subsequently, 20 ml fresh medium was added, and the cells were incubated at 37˚C in a humidified atmosphere containing 5% $CO_2$ for an additional 48-72 h. The supernatant from the 293T cells was then collected, centrifuged at 4,000 x g for 10 min at 4˚C to remove cell debris and filtered through a 0.45-$\mu$m filter. The supernatant was then centrifuged at 25,000 x g for 2 h at 4˚C; after centrifugation, the supernatant was discarded, and viral storage solution was added to completely dissolve the lentiviral particles. For cell transduction, HCT116 and RKO cells were subcultured, seeded into 12-well plates at a density of $0.4x10^5$ cells/well and were cultured overnight. Lentivirus coding shRNA targeting FGGY (LV-FGGY-RNAi; hU6-MCS-Ubiquitin-EGFP-IRES-puromycin) or the control shRNA (sh-Ctrl; hU6-MCS-Ubiquitin-EGFP-IRES-puromycin) (18) was added at a multiplicity of infection (MOI) of 10, with medium and Hitrans P infection enhancement reagent (cat. no. REVG005; Shanghai GeneChem Co., Ltd.) reaching a total volume of 500 $\mu$l/well. The specific sequences of these shRNAs are detailed in Table SIV. The medium was changed after 12 h of transduction and fresh medium was added. The cells were then incubated at 37˚C in a humidified atmosphere containing 5% $CO_2$ for an additional 72 h. After 72 h, the infection efficiency was verified by observing the number of GFP-positive cells under a fluorescence microscope. To confirm the knockdown of FGGY, the mRNA and protein expression levels of FGGY were assessed using RT-qPCR and western blot analysis, respectively. After verifying a significant decrease in FGGY expression at both the mRNA and protein levels, the cells were collected for subsequent experiments.

To investigate the effects of FGGY overexpression on cell proliferation, HT-29 cells were transduced with a lentiviral vector (GV492; Ubi-MCS-3FLAG-CBh-gcGFP-IRES-puromycin) (MOI, 10) that encoded the full-length human FGGY gene [NCBI Gene ID: 55277; OBiO Technology (Shanghai) Corp., Ltd.] or an empty vector control (GV492 without FGGY insert) at the same MOI. The protocol for the overexpression plasmid transduction was the same as that described for shRNA transduction. The medium was changed after 12 h of transduction and fresh medium was added. The cells were then incubated at 37˚C in a humidified atmosphere containing 5% $CO_2$ for an additional 72 h. After 72 h, the infection efficiency was verified by observing the number of GFP-positive cells under a fluorescence microscope. Successfully transduced cells were selected using 2 $\mu$g/ml puromycin (cat. no. A1113803; Thermo Fisher Scientific, Inc.) for 1 week, and then maintained in medium containing 1 $\mu$g/ml puromycin. To confirm the overexpression of FGGY, the mRNA and protein expression levels of FGGY were assessed using RT-qPCR and western blot analysis, respectively. After verifying a significant decrease in FGGY expression at both the mRNA and protein levels, the cells were collected for subsequent experiments.

*Western blot analysis*. After lentiviral transduction and puromycin selection, cells were collected and lysed using RIPA lysis buffer (Beyotime Institute of Biotechnology) supplemented with 1 mM PMSF and protease inhibitors. The total protein concentration was determined using the Pierce BCA Protein Assay Kit (Thermo Fisher Scientific, Inc.). Protein lysates (50 $\mu$g) were separated by SDS-PAGE on 10% gels and were then transferred onto polyvinylidene difluoride membranes. These membranes were subsequently blocked with 5% nonfat milk in TBS-0.1% Tween for 2 h at room temperature, and then incubated with primary

antibodies against FGGY (cat. no. PA5-120316; Thermo Fisher Scientific, Inc.), p53 (cat. no. 10442-1-AP; Proteintech Group, Inc.), p21 (cat. no. 2947S; Cell Signaling Technology, Inc.), PCNA (cat. no. 10205-2-AP; Proteintech Group, Inc.), Bcl-2 (cat. no. 3498; Cell Signaling Technology, Inc.), Bax (cat. no. 2772; Cell Signaling Technology, Inc.) or GAPDH (cat no. Abp57259; Abbkine Scientific Co., Ltd.) (all at a dilution of 1:1,000) at 4˚C overnight. This was followed by incubation with goat anti-rabbit secondary antibodies conjugated with horseradish peroxidase (1:5,000; cat. no. 7074; Cell Signaling Technology, Inc.) for 2 h at room temperature. Protein bands were detected using an ECL imager (cat no. 32209; Thermo Fisher Scientific, Inc.) and their intensities were analyzed with ImageLab software (version 5.2.1; Bio-Rad Laboratories, Inc.). GAPDH expression was used as a loading control. Each experiment was performed in triplicate.

*Cell viability assay*. The cells were seeded in 96-well plates at a density $0.2x10^5$/ml and were cultured for 24, 48, 72, 96 or 120 h, after which 10 $\mu$l CCK-8 solution (cat. no. KTA1020; Abbkine Scientific Co., Ltd.) was added to each well. The plates were then incubated at 37˚C for 2 h in an incubator with 5% $CO_2$ in the dark. Subsequently, the optical density of each well was measured at an absorbance of 450 nm using a microplate reader.

*Cell cycle and apoptosis analyses*. For the cell cycle analysis, transduced cells were harvested and fixed in 70% ethanol at 4˚C overnight. These fixed cells were then centrifuged at 2,000 x g for 3 min at room temperature, washed and incubated with FxCycle™ PI/RNase staining solution (cat no. F10797; Thermo Fisher Scientific, Inc.) for 30 min at room temperature. Cell cycle progression was analyzed using a FACSCalibur flow cytometer (BD Biosciences), with Modfit LT version 3.0 software (Verity Software House, Inc.). For the apoptosis analysis, transfected cells were rinsed twice with ice-cold PBS and incubated with Annexin-V-AbFluor™ 647 Apoptosis Detection Kit (Abbkine Scientific Co., Ltd.) for 30 min at 37˚C in the dark. The rate of apoptosis in these cells was also determined using FACSCalibur flow cytometer (BD Biosciences). Data were analyzed using CellQuest Pro software (version 6.0; BD Biosciences). Each assay was conducted in triplicate.

*Colony formation assay*. Transduced cells were seeded in 12-well plates at a density of 500 cells/well and were incubated at 37˚C in a 5% $CO_2$ atmosphere for 10 days. At the end of this incubation period, the cells were fixed using 4% paraformaldehyde for 15 min at room temperature and were subsequently stained with 0.1% crystal violet for 15-20 min at room temperature. Colonies were defined as clusters containing ≥50 cells and were observed using a light microscope (Leica Microsystems GmbH) and images were captured with a camera. The colonies were manually counted and the relative change in colony formation was determined. Data were normalized to the control group. Each assay was conducted in triplicate.

*Xenograft experiments in nude mice*. A total of 22 male BALB/c nude mice (age, 6-8 weeks; weight, 20-22 g) were acquired from Shanghai SLAC Laboratory Animal Co. Ltd. The mice were housed in a controlled, pathogen-free environment, with a stable temperature (22˚C), humidity (40-70%) and under a 12-h light/dark cycle. The mice were provided unrestricted access to food and water. All experimental procedures involving animals were approved by the Institutional Animal Care and Use Committee of the Fujian University of Traditional Chinese Medicine (approval no. FJTCM IACUC 2019052) and were conducted in strict accordance with international guidelines (19) for the ethical use of animals in research.

Transduced HCT116, RKO and HT-29 cells ($1x10^6$) in 100 $\mu$l medium mixed with 50% Matrigel were subcutaneously injected into the flank of nude mice (n=5, sh-FGGY and sh-Ctrl groups; or n=6, FGGY overexpression and control groups). Tumor growth was monitored every other day using a vernier caliper, with the volume calculated as: 1/2 (larger diameter x smaller diameter$^2$). At the end of the experimental time point (16 days post-inoculation for shRNA groups and 20 days post-inoculation for overexpression groups), the mice were anesthetized using 2% isoflurane inhalation for induction and 1.5% isoflurane inhalation for maintenance. Tumor imaging was captured using the IVIS Spectrum live-animal imaging system (PerkinElmer, Inc.). Signal intensity was quantified based on the photon count per second from the region of interest. After imaging, the mice were sacrificed by cervical dislocation, and the tissues were harvested for further analysis.

*Isobaric tags for relative and absolute quantitation (iTRAQ) analysis and protein identification*. iTRAQ analysis was used to screen differentially expressed proteins (DEPs) after knockdown of FGGY in HCT116 cells (20,21). The protein samples were reduced with 10 mM DTT at 56˚C for 1 h and alkylated with 55 mM IAM in the dark for 1 h at room temperature. The protein samples were then digested overnight at 37˚C with sequencing-grade modified trypsin (Promega Corporation) at a protein-to-trypsin ratio of 20:1. After trypsin digestion, peptides were dried by vacuum centrifugation (10,000 x g, 2 h, 45˚C) and reconstituted in 0.5 M TEAB. The liquid chromatography (LC)-MS/MS analysis was performed by CapitalBio Technology Co., Ltd. using a Q Exactive mass spectrometer (Thermo Fisher Scientific, Inc.). The peptide separation was achieved by reversed-phase chromatography on a DIONEX nano-UPLC system, using an Acclaim C18 PepMap100 nano-Trap column (75 $\mu$m x 2 cm) connected to an Acclaim PepMap RSLC C18 analytical column (75 $\mu$m x 25 cm, 2 $\mu$m particle size) (all from Thermo Fisher Scientific, Inc.). Before loading, the sample was dissolved in mobile phase A, which consisted of 2% acetonitrile and 0.1% formic acid. A linear gradient of mobile phase B (0.1% formic acid in 99.9% acetonitrile) was applied, increasing from 2 to 35% over 45 min, followed by a sharp increase to 80% mobile phase B in 1 min, at a flow rate of 300 nl/min. The nano-LC was coupled online with the Q Exactive mass spectrometer using a stainless-steel emitter attached to a nanospray ion source. Nitrogen gas temperature was 0.6 Mpa and nebulizer pressure was 50 psi. MS analysis was performed in a data-dependent manner, with full scans (350-1,600 m/z) acquired using an Orbitrap mass analyzer (Thermo Fisher

Scientific, Inc.) at a mass resolution of 70,000 at 400 m/z in Q Exactive. The 20 most intense precursor ions from each survey scan were selected for MS/MS analysis, which was performed at a mass resolution of 17,500 at 400 m/z in the Orbitrap analyzer. All tandem mass spectra were generated using the higher-energy collision dissociation method, with a dynamic exclusion of 20 sec. Proteins with >1.2-fold change in expression between groups and with a P-value of <0.05 were identified as DEPs. These DEPs were identified using volcano plots and further analyzed using hierarchical clustering plots in R software (version 4.1.0; R Foundation for Statistical Computing; https://www.R-project.org/) using the ggplot2 package (version 3.3.5; https://cran.r-project.org/web/packages/ggplot2/) for volcano plots and pheatmap package (version 1.0.12; https://cran.r-project.org/web/packages/pheatmap/) for hierarchical clustering analysis. To ascertain the biological pathways affected by these DEPs, Kyoto Encyclopedia of Genes and Genomes (KEGG) pathway, Reactome pathway and PANTHER pathway analyses were performed (22-24). The enriched pathways were identified from the DEPs using KEGG database (https://www.genome.jp/kegg/) with a significance cutoff of P<0.05 (25,26).

*Phosphoproteome analysis and phosphopeptide identification*. Transduced cells were lysed using SDT lysis buffer (Beyotime Institute of Biotechnology). Proteins were then digested with trypsin using filter-aided sample preparation. A total of 100 $\mu$g peptide mixture from each sample was labeled using iTRAQ reagent (SCIEX) adhering to the manufacturer's guidelines. Phosphopeptide enrichment was carried out, followed by LC-MS/MS analysis as per the manufacturer's instruction (L-3000 HPLC system; RIGOL Technologies) (27,28). Subsequently, identification and quantification of phosphorylated proteins were achieved using the MASCOT engine (version 2.2; Matrix Science), integrated into Proteome Discoverer 2.4.

Motif analysis was carried out using MeMe (http://meme-suite.org/). The amino acid sequences containing the modified site, and six upstream/downstream amino acids from the modified site (resulting in a total of 13 amino acid positions), were extracted and used for motif prediction (parameters used: Width, 13; occurrences, 20; background, species). Phosphopeptide sequences were analyzed with InterProScan software (version 5.52-86.0; EMBL-EBI)to identify protein domain signatures from the InterPro member database Pfam (22,23). Phosphopeptides showing ≥1.2-fold difference in expression in comparative analyses and with a P-value of <0.05 were considered differentially expressed. These phosphopeptides were visualized using volcano plots and further analyzed using hierarchical clustering plots. Proteins were categorized based on their KEGG annotations with P<0.05.

*Senescence β-galactosidase (SA-β-gal) staining*. Cells with knockdown of FGGY or overexpression of FGGY were first washed with 1xPBS, and subsequently fixed with 4% paraformaldehyde for 10-15 min at room temperature. After fixation, the cells were washed and then incubated with β-gal staining solution (cat no. ab102534; Abcam) in a dry incubator at 37˚C overnight. Images of the β-gal stained-cells were captured using a light microscope (Leica Microsystems GmbH) at a x200 magnification. Each assay was conducted in triplicate.

*Immunofluorescence staining*. Cells were initially rinsed with PBS after knockdown of FGGY, and were then fixed in 4% paraformaldehyde for 20 min at room temperature. The cells were subsequently permeabilized with 0.1% Triton X-100, blocked with 1% BSA (cat. no. SW3015; Beijing Solarbio Science & Technology Co., Ltd.) for 1 h at room temperature, and were incubated overnight at 4˚C with primary antibodies against HP1γ (cat. no. 2619; Cell Signaling Technology, Inc.), or trimethylation of H3K9 (H3k9me3; cat. no. 49-1008; Thermo Fisher Scientific, Inc.), at a dilution of 1:200. Post-primary antibody incubation, the cells were washed with PBS and incubated with Goat anti-Rabbit IgG Alexa Fluor™ 647 (cat. no. A-21245; Thermo Fisher Scientific, Inc.) at a dilution of 1:200 for 1 h at room temperature, followed by Hoechst 33342 staining for 10 min at room temperature. All images were captured using a fluorescence microscope (Leica Microsystems GmbH) at a magnification of x400. Each assay was conducted in triplicate.

*Statistical analysis*. Experiments were performed at least in triplicate and data are presented as the mean ± standard deviation. Statistical analysis was conducted using SPSS 26.0 software (IBM Corp). Comparisons between two datasets were made using a two-tailed unpaired Student's t-test for normally distributed data or Mann Whitney-U test for non-parametric data. Multiple group comparisons were analyzed using one-way ANOVA followed by Tukey's post hoc test or two-way ANOVA followed by Bonferroni's post hoc test. The associations between FGGY protein expression and clinicopathological characteristics were analyzed using $\chi^2$ test or Fisher's exact test (when the expected counts were ≤5 in >20% of samples) for categorical variables. The correlation between genes was analyzed using Pearson correlation coefficient. P<0.05 was considered to indicate a statistically significant difference.

## Results

*Upregulation of FGGY expression in CRC is associated with shorter overall survival and metastasis in patients with CRC*. The mRNA and protein expression levels of FGGY in various types of digestive system neoplasms were determined by GEPIA database analysis and TMA analysis in COAD, READ, PAAD, ESCA, STAD and LIHC. There was an elevation in FGGY mRNA and protein expression in PAAD, COAD and READ tissues compared with in normal tissues from healthy controls (Fig. 1A-F). This increase was also observed in COAD and READ tissues compared with in adjacent noncancerous tissues (Fig. 1A-D). However, FGGY protein expression did not exhibit significant differences in ESCA, STAD and LIHC tissues compared with in normal tissues from healthy controls and adjacent noncancerous tissues (Fig. 1G-L). These findings suggested that FGGY could serve as a potential specific marker of CRC, with increased expression in CRC.

Furthermore, the analysis of TCGA and GEO datasets (GSE20916 and GSE13513) further confirmed the upregulation of FGGY mRNA expression in CRC tissues compared

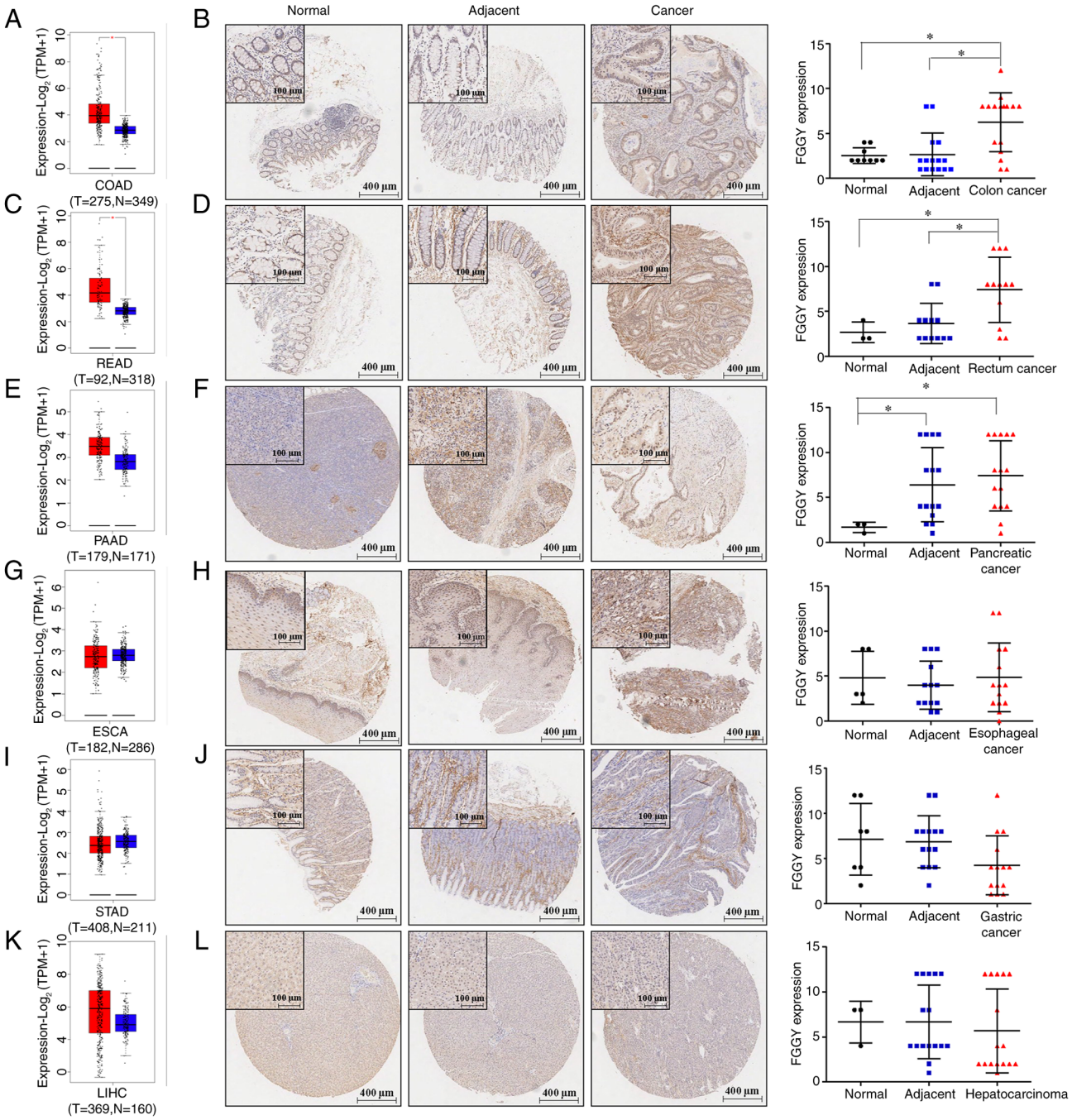


Figure 1. FGGY expression at both mRNA and protein levels in various type of cancer tissues. FGGY expression was analyzed in (A) COAD, (C) READ, (E) PAAD, (G) ESCA, (I) STAD and (K) LIHC from the Gene Expression Profiling Interactive Analysis database. FGGY expression was analyzed in (B) COAD, (D) READ, (F) PAAD, (H) ESCA, (J) STAD and (L) LIHC from the tissue microarray. *P<0.05. COAD, colon adenocarcinoma; ESCA esophageal cancer; FGGY, FGGY carbohydrate kinase domain containing; LIHC, liver hepatocellular carcinoma; N, normal; PAAD, pancreatic cancer; READ, rectal adenocarcinoma; STAD, gastric cancer; T, tumor; TPM, transcripts per million.

with in adjacent normal tissues (Fig. 2A-C). This finding was further verified at the mRNA level using a cDNA array by RT-qPCR analysis (Fig. 2D; n=15 pairs) and at the protein level using a TMA via IHC analysis (Fig. 2E; n=71 pairs) in CRC tissues compared with in adjacent normal tissues. Moreover, survival analysis revealed an association between high FGGY protein expression and shorter overall survival in patients with CRC (Fig. 2F; high expression, n=71; low expression, n=23; cutoff, 3). Analysis of the association of FGGY with clinicopathological characteristics revealed that higher FGGY expression was associated with N stage in patients with CRC (Table I).

*FGGY knockdown inhibits cell viability and induces cell apoptosis in vitro*. Given that the endogenous expression levels of FGGY were relatively high in HCT116 and RKO cells, but low in HT-29 cells (Fig. S1A), the present study chose to knock down FGGY in HCT116 and RKO cells, and to overexpress FGGY in HT-29 cells. To investigate the role of FGGY in CRC cell viability, three distinct shRNAs

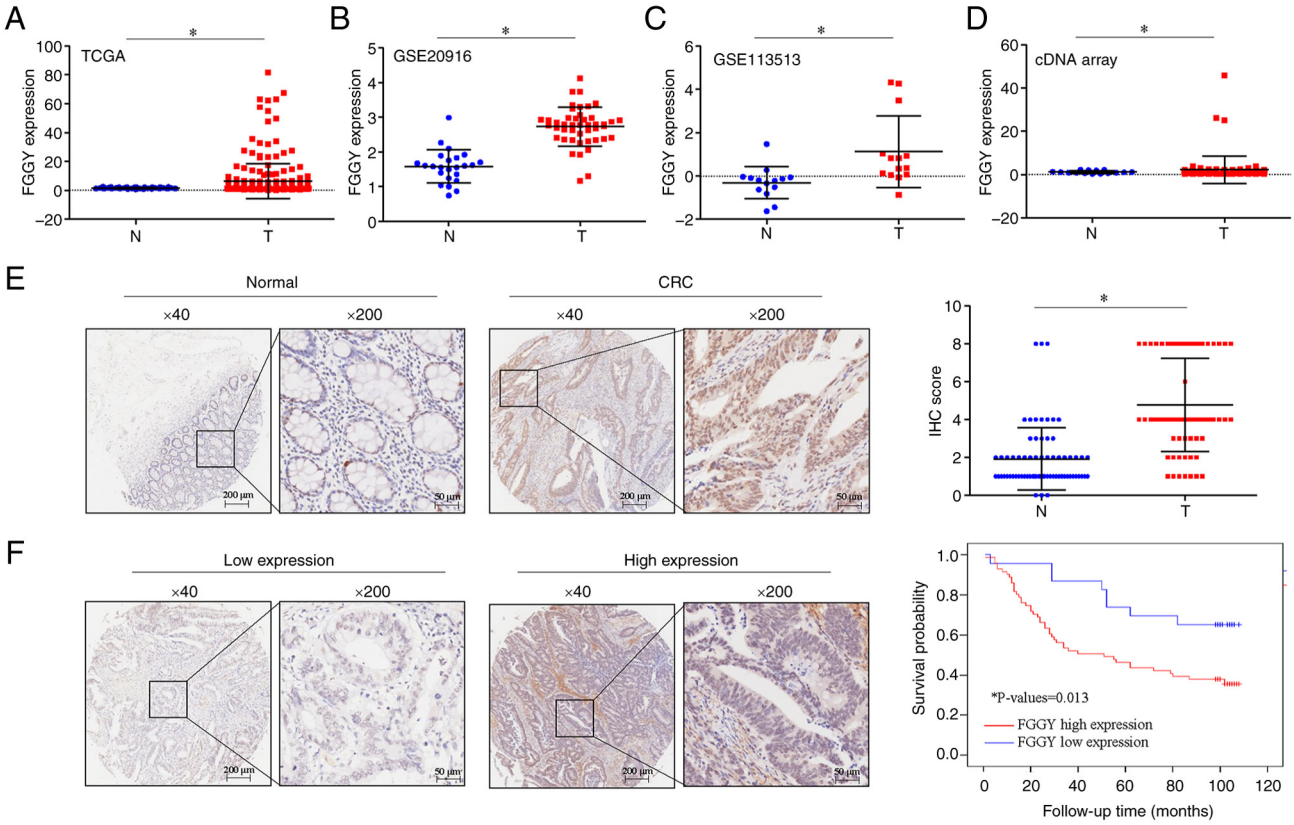


Figure 2. FGGY expression at both mRNA and protein levels in CRC tissues. FGGY mRNA expression in CRC tissues and N tissues from (A) TCGA. FGGY mRNA expression in CRC tissues and N tissues from Gene Expression Omnibus (B) GSE20916 and (C) GSE113513 datasets. (D) FGGY mRNA expression labels in CRC tissues (n=80) and N tissues (n=15) on the CRC cDNA chip were analyzed by quantitative PCR. GAPDH was used as an internal control. (E) FGGY protein expression in CRC T tissues and N tissues, as determined by IHC of the tissue microarray. Representative images were taken at a magnification of x40 or x200 (right panel); the IHC score was calculated as intensity score x percentage score (left panel). (F) Kaplan-Meier plots of survival of patients with CRC, stratified by FGGY protein expression based on tissue microarray. *P<0.05. CRC, colorectal cancer; FGGY, FGGY carbohydrate kinase domain containing; IHC, immunohistochemistry; N, non-cancerous; TCGA, The Cancer Genome Atlas; T, tumor.

specifically targeting FGGY were utilized, which were encoded into lentiviruses for cell transduction. Compared with in the sh-Ctrl group, transducing HCT116 cells with these shRNAs significantly reduced FGGY expression at both the mRNA and protein levels (Fig. S1B and C), and decreased cell viability (Fig. S1D). Since all three shRNAs exhibited a comparable effect on FGGY expression and cell viability, further experiments were conducted with a single construct, designated as sh-FGGY (specifically, sh-FGGY-1). RT-qPCR and western blot analysis confirmed a substantial decrease in FGGY expression at both the mRNA and protein levels in HCT116 and RKO cells after transduction with sh-FGGY (Fig. 3A and B). Additionally, FGGY knockdown significantly reduced the number of colonies formed and cell viability (Fig. 3C and D). Furthermore, FGGY knockdown resulted in an increased proportion of cells at the $G_0/G_1$ phase and a decreased proportion of cells at the S phase in both HCT116 and RKO cells (Fig. 3E). Moreover, Annexin V staining and subsequent flow cytometric analysis revealed that FGGY knockdown significantly elevated the percentage of early apoptotic cells (Fig. 3F). Additionally, FGGY knockdown increased the expression levels of the pro-apoptotic protein Bax and decreased the expression levels of anti-apoptotic Bcl-2 in HCT116 cells (Fig. S2). By contrast, HT-29 cells transduced with lentiviral vectors designed to overexpress FGGY exhibited elevated FGGY protein expression and increased cell viability (Fig. S3A and B).

*FGGY knockdown suppresses CRC tumor growth in vivo.* Analysis of tumor growth *in vivo* using a xenograft mouse model revealed that, compared with in the sh-Ctrl group, FGGY knockdown significantly inhibited CRC tumor growth in nude mice, as indicated by a marked reduction in tumor volume (Fig. 4A), fluorescence intensity of tumor cells (Fig. 4B) and tumor weight (Fig. 4C). By contrast, overexpression of FGGY significantly promoted CRC tumor growth in nude mice, as evidenced by an increase in tumor volume (Fig. S3C), fluorescence intensity of tumor cells (Fig. S3D) and tumor weight (Fig. S3E) in nude mice.

*FGGY knockdown in CRC cells modulates the expression of multiple proteins/phosphopeptides and enriches multiple pathways.* To further explore the possible mechanisms by which FGGY knockdown inhibits tumor growth in CRC, iTRAQ and phosphoproteomics analyses were employed to identify DEPs in HCT116 cells after FGGY knockdown. As shown in Fig. 5, a total of 809 DEPs were identified, which included 236 proteins with increased expression and 573 with decreased expression (fold change >1.2, P<0.05) using iTRAQ methodology (Fig. 5A and B; Tables SV and SVI). Additionally, phosphoproteomics

Table I. Association between FGGY expression and the clinicopathological characteristics of patients with colorectal cancer in a tissue microarray.

| | | FGGY protein expression | | |
|---|---|---|---|---|
| Variable | Total (n=94) (%) | Low expression (n=23) (%) | High expression (n=71) (%) | P-value |
| Age | | | | 0.280 |
| ≤65 years | 42 (44.7) | 12 (12.8) | 30 (31.9) | |
| >65 years | 52 (55.3) | 11 (11.7) | 41 (43.6) | |
| Sex | | | | 0.554 |
| Male | 52 (55.3) | 15 (16.0) | 37 (39.4) | |
| Female | 42 (44.7) | 8 (8.5) | 34 (36.2) | |
| Pathological stage | | | | 0.495 |
| I | 5 (5.3) | 1 (1.1) | 4 (4.3) | |
| II | 78 (83.0) | 21 (22.3) | 57 (60.6) | |
| III | 11 (11.7) | 1 (1.1) | 10 (10.6) | |
| Tumor size | | | | 0.389 |
| ≤5 cm | 48 (51.1) | 15 (16.0) | 33 (35.1) | |
| >5 cm | 46 (48.9) | 8 (8.5) | 38 (40.4) | |
| T stage | | | | 0.498 |
| T1 | 1 (1.1) | 0 (0) | 1 (1.1) | |
| T2 | 5 (5.3) | 0 (0) | 5 (5.3) | |
| T3 | 71 (75.5) | 21 (22.3) | 50 (53.2) | |
| T4 | 13 (13.8) | 2 (2.1) | 11 (11.7) | |
| N stage | | | | 0.042[a] |
| N0 | 56 (59.6) | 17 (18.%) | 39 (41.5) | |
| N1 | 27 (28.7) | 6 (6.4) | 21 (22.3) | |
| N2 | 11 (11.7) | 0 (0) | 11 (11.7) | |
| M stage | | | | >0.999 |
| M0 | 91 (96.8) | 22 (23.4) | 69 (73.4) | |
| M1 | 3 (3.2) | 1 (1.1) | 2 (2.1) | |

[a]P<0.05 indicate statistical significance determined using $\chi^2$ test. FGGY, FGGY carbohydrate kinase domain containing.

analysis identified 304 differentially expressed phosphopeptides, comprising 145 upregulated and 159 downregulated phosphopeptides (fold change >1.2, P<0.05) (Fig. 5D and E; Tables SVII and SVIII). The KEGG pathway enrichment analysis revealed that these proteins and phosphopeptides were enriched in various signaling pathways (Fig. 5C and F; Tables SIX and SX). KEGG analysis of iTRAQ revealed enrichment in both the 'Formation of senescence-associated heterochromatin foci (SAHF)' and the 'Senescence-associated secretory phenotype (SASP)' (Fig. 5C). These findings suggested that cellular senescence may serve a significant role in the effects of FGGY knockdown. Additionally, KEGG analysis of phosphoproteomics analysis revealed enrichment in both the 'p53 pathway' and 'p53 signaling pathway' (Fig. 5F). Given the well-established link between cellular senescence and the p53 pathway, the present study further investigated these two processes. Both cellular senescence and the p53 pathway are known to regulate cell death and tumor suppression, indicating that FGGY may modulate the p53 signaling pathway and influence cell senescence.

*FGGY knockdown promotes CRC cell senescence through the p53/p21 pathway*. The present study aimed to elucidate how FGGY knockdown regulates cell senescence and the p53 pathway in CRC. Correlation analysis of microarray expression data from the GEO and TCGA databases revealed that a weak negative correlation existed between FGGY and p53 expression (Fig. 6A and B). Compared with in the control group, FGGY knockdown led to an increase in the protein expression levels of p53 and p21, while the expression levels of PCNA were decreased (Fig. 6C). Notably, when comparing the two cell lines, the inhibitory effects of FGGY knockdown on the viability of HCT116/p53$^{+/+}$ cells were attenuated in HCT116/p53$^{-/-}$ cells (Fig. 6D and E). By contrast, HT-29 cells transduced with lentiviral vectors designed to overexpress FGGY exhibited decreased p53 and p21 protein expression compared with that in cells transduced with control vectors (Fig. S3F).

Cellular senescence is characterized by increased SA-β-gal activity, reduced cell proliferation, cell cycle arrest and the

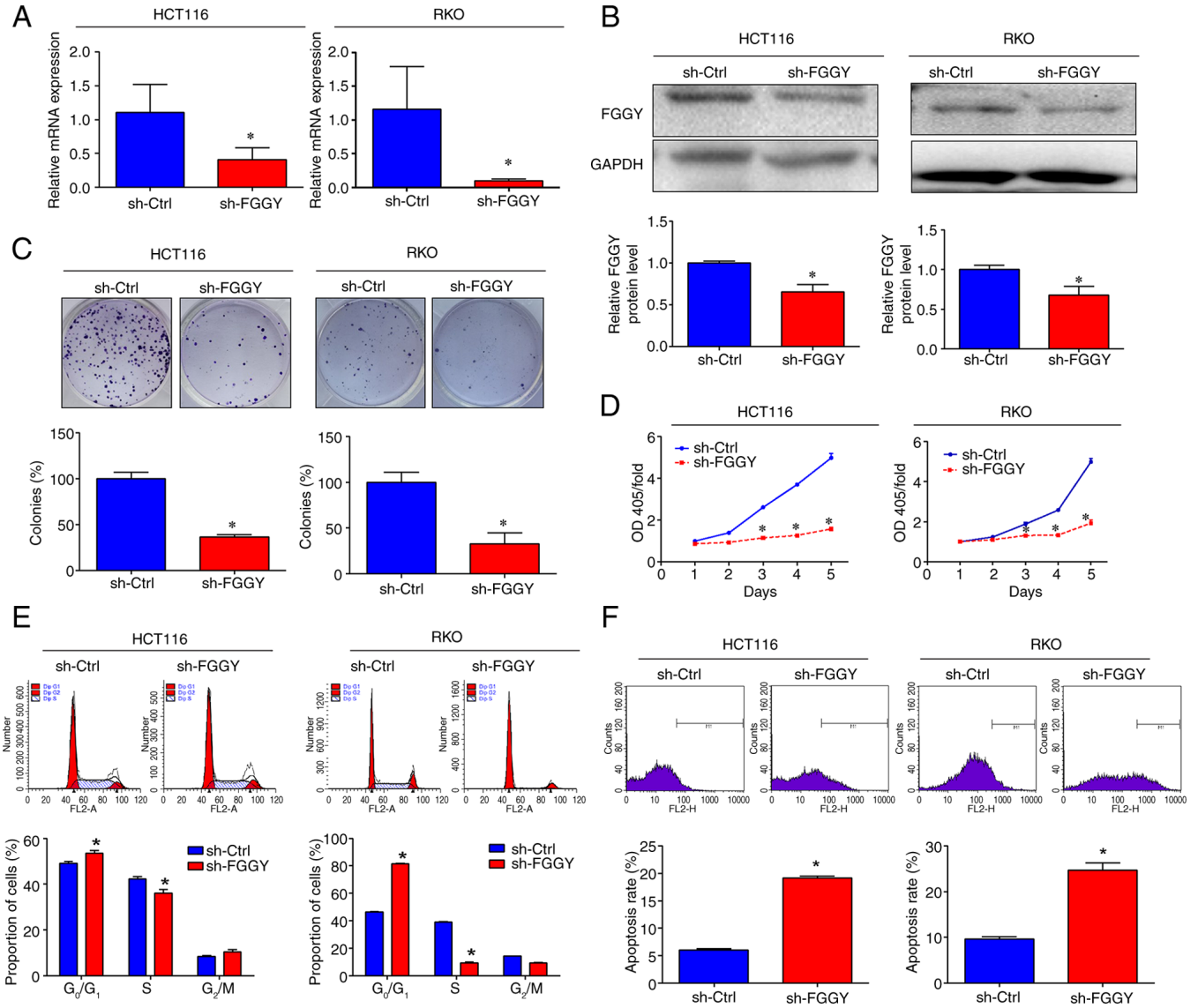


Figure 3. FGGY knockdown inhibits the proliferation of colorectal cancer cells. (A) mRNA and (B) protein expression levels of FGGY in HCT116 and RKO cells after transduction with sh-FGGY or sh-Ctrl was assessed by quantitative PCR and western blotting. GAPDH was used as a loading control. Band intensities were semi-quantified using ImageLab software. (C) Colony formation of HCT116 and RKO cells transduced with sh-FGGY or sh-Ctrl was assessed by colony formation assay. Colony formation was normalized to the sh-Ctrl group. (D) Viability of HCT116 and RKO cells after FGGY knockdown was determined by Cell Counting Kit-8. Data were normalized to viability at day 1 and presented as fold change. (E) Percentage of HCT116 and RKO cells transduced with sh-FGGY or sh-Ctrl in $G_0/G_1$, S and $G_2/M$ phases, as determined by flow cytometry. Representative flow cytometry plots and the percentage of cells at each stage are shown. (F) Apoptosis of HCT116 and RKO cells was detected by Annexin V staining and flow cytometric analysis. Representative plots and percentages of apoptotic cells are shown. *P<0.05 vs. sh-Ctrl. Ctrl, control; FGGY, FGGY carbohydrate kinase domain containing; OD, optical density; sh, short hairpin.

formation of SAHF (29-31). To further investigate the potential regulatory effects of FGGY on senescence, a SA-β-gal activity assay was conducted in both HCT116/$p53^{+/+}$ and HCT116/$p53^{-/-}$ cells. The results revealed that β-gal activity was significantly increased after FGGY knockdown in HCT116/$p53^{+/+}$ cells, but β-gal activity remained unchanged after FGGY knockdown in HCT116/$p53^{-/-}$ cells (Fig. 6F). Conversely, β-gal activity was decreased in HT-29 cells after FGGY overexpression (Fig. S3G). Moreover, FGGY knockdown significantly upregulated the expression of cell senescence markers HP1γ and H3k9me3m in HCT116/$p53^{+/+}$ cells, whereas in HCT116/$p53^{-/-}$ cells, FGGY knockdown did not affect the protein expression of cell senescence markers HP1γ and H3K9me3 (Fig. 6G and H).

## Discussion

In the present study, FGGY protein expression was significantly upregulated in COAD and READ tissues compared with that in normal tissues from healthy controls and adjacent noncancerous tissues, and it was elevated in PAAD tissues compared with that in normal tissues from healthy controls. However, there were no significant differences in FGGY expression between tumor and adjacent noncancerous tissues in ESCA, STAD and LIHC.

In addition, higher levels of FGGY in CRC tissues were closely associated with advanced N stage, as well as shorter overall survival of patients with CRC. These findings indicated that FGGY may serve as a potential biomarker specific

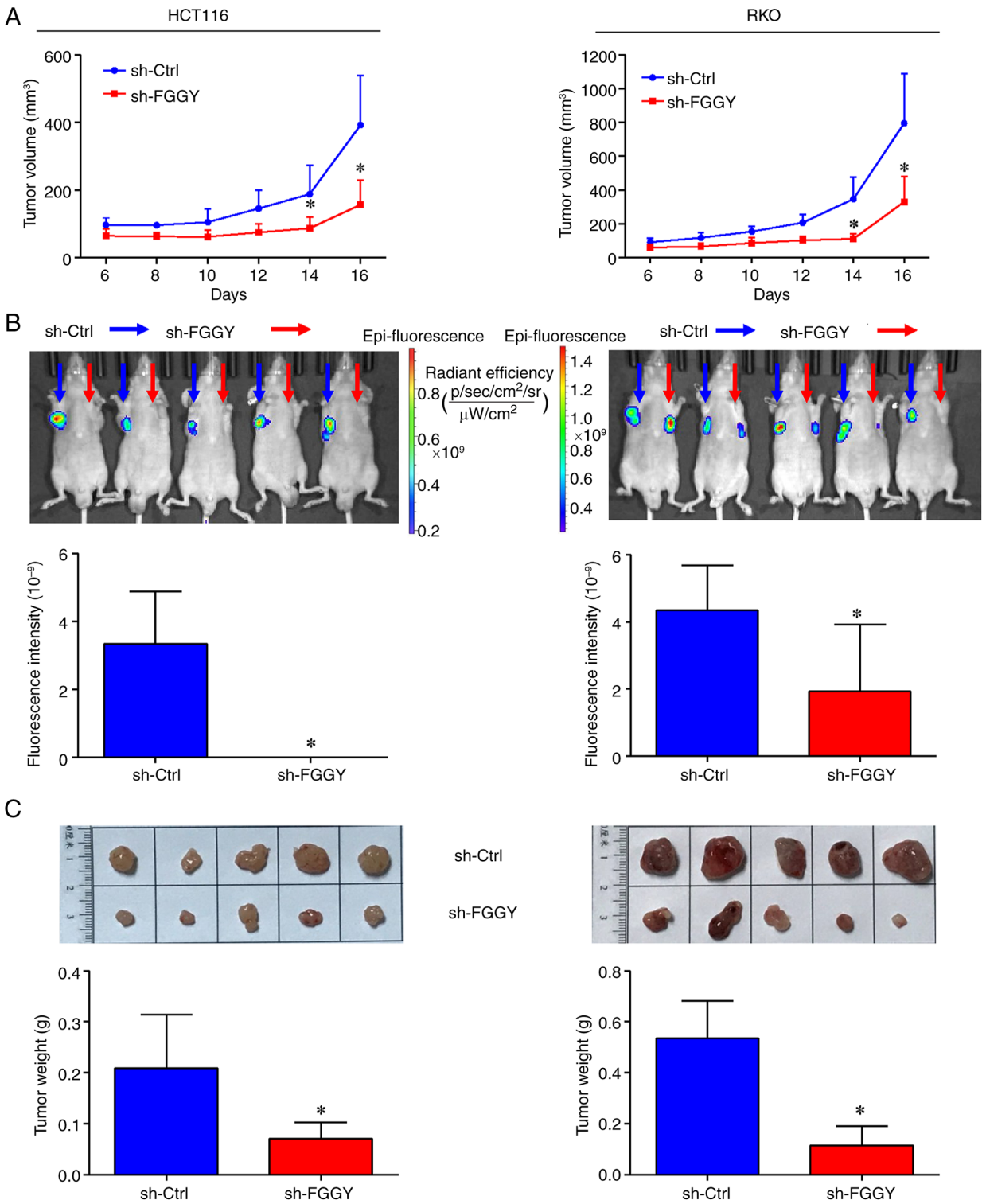


Figure 4. FGGY knockdown inhibits colorectal cancer cell growth *in vivo*. A xenograft nude mouse model was established to investigate the tumor growth of HCT116 and RKO cells *in vivo*. A total of 1.0x10$^6$ cells transduced with lentiviruses encoding sh-Ctrl or sh-FGGY were injected subcutaneously into the forelimb axillae (sh-Ctrl, left; sh-FGGY, right) of BALB/c nude mice. (A) Tumor volumes, (B) fluorescence intensities of tumor cells, and (C) images of tumors and tumor weights were determined and recorded. *P<0.05 vs. sh-Ctrl. Ctrl, control; FGGY, FGGY carbohydrate kinase domain containing; sh, short hairpin.

for CRC, distinguishing it from other types of digestive system neoplasms. Functional studies revealed that FGGY knockdown significantly suppressed CRC growth by inhibiting cell viability and inducing cell apoptosis through the modulation of multiple targets and pathways. Notably, verification of the potential targets and pathways revealed that FGGY knockdown triggered cell senescence through activation of the p53/p21 signaling pathways, indicating a promising direction for developing novel anti-CRC therapeutic strategies.

FGGY is a gene that encodes a kinase from the FGGY kinase family, which are recognized as phosphotransferases (6). A previous study linked its expression with an

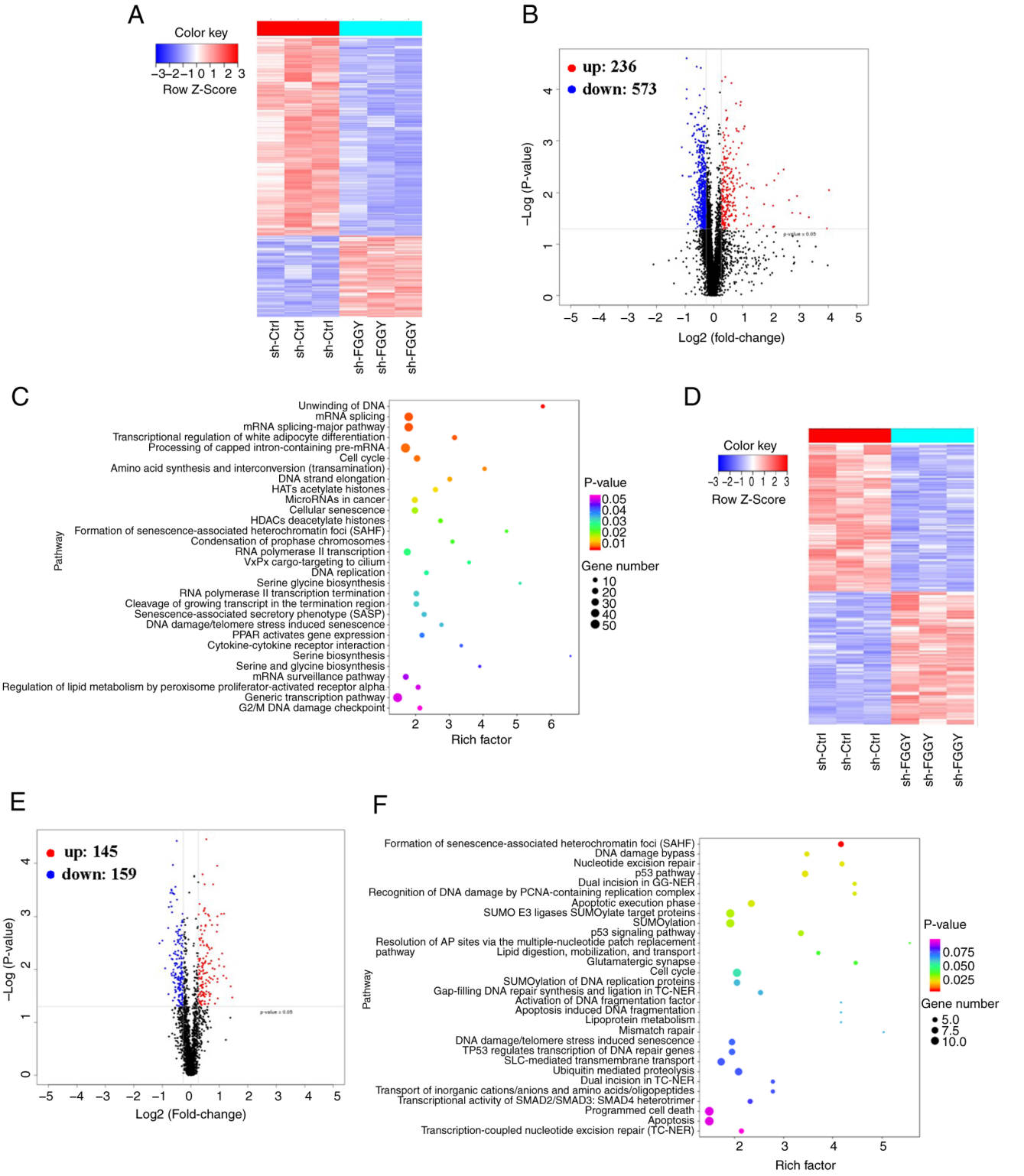


Figure 5. Cancer-associated pathways were significantly enriched among proteins dysregulated by FGGY knockdown in HCT116 cells. HCT116 cells were transduced with lentiviruses encoding sh-FGGY or sh-Ctrl, and (A-C) isobaric tags for relative and absolute quantitation and (D-F) phosphoproteomics analyses were used to identify DEPs. (A and D) Hierarchical clustering plots and (B and E) volcano plots were used to identify DEPs (fold change >1.2, P<0.05). (C and F) KEGG pathway enrichment analysis was performed to identify functionally related gene pathways. The top 30 enriched signaling pathways are shown. Ctrl, control; DEPs, differentially expressed proteins. FGGY, FGGY carbohydrate kinase domain containing; sh, short hairpin.

increased risk of sporadic amyotrophic lateral sclerosis (8). To the best of our knowledge, the present study is the first to reveal an elevation in FGGY expression at both mRNA and protein levels in CRC (including COAD and READ) tissues, compared with those in normal tissues from healthy controls and adjacent noncancerous tissues, which was associated with poorer prognosis and CRC progression. Notably, analysis of TCGA data showed that FGGY expression levels were not significantly different among normal tissues, adjacent non-tumor tissues and tumor tissues in other digestive system

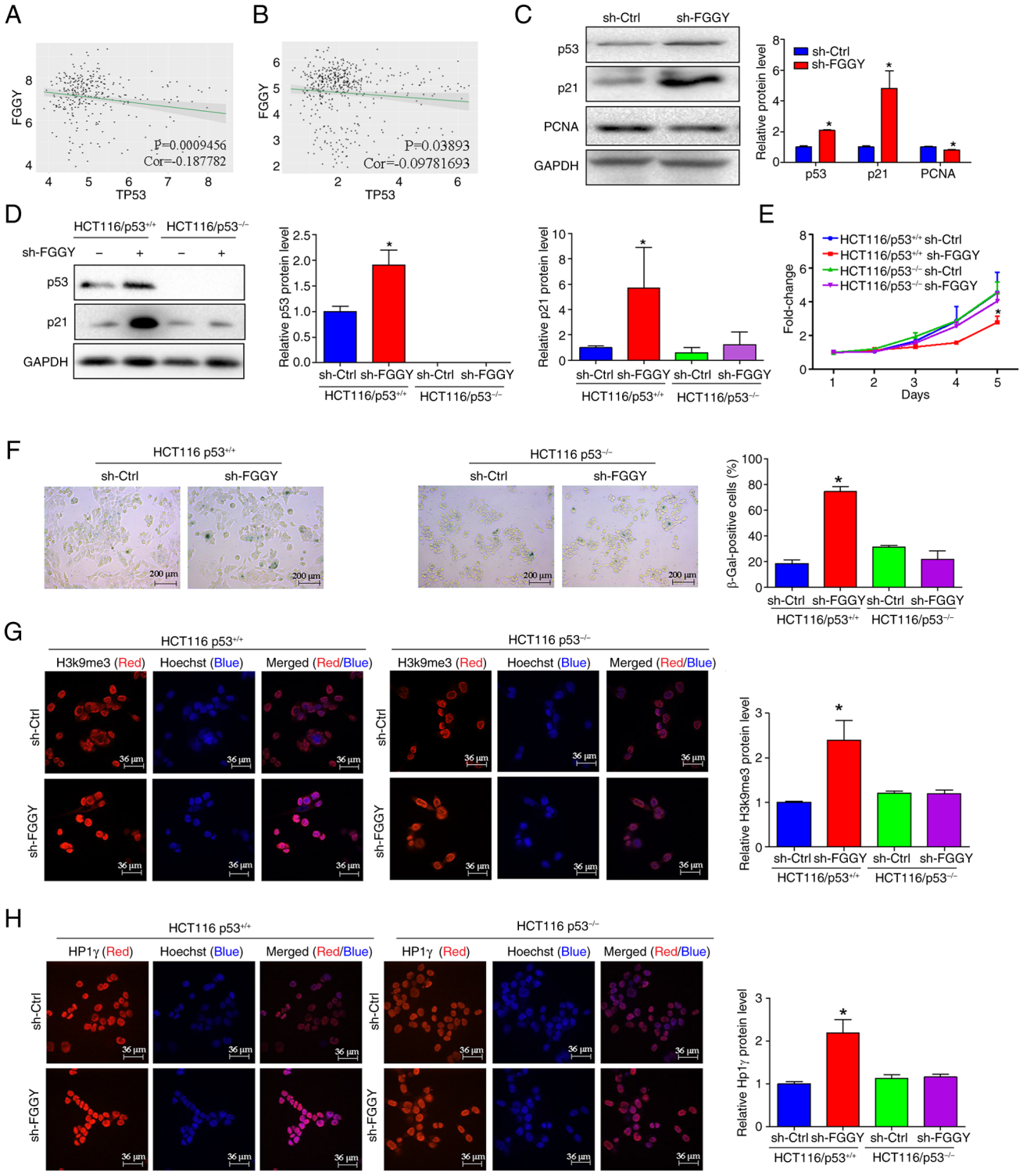


Figure 6. FGGY knockdown promotes cell senescence by activating the p53 pathway. The correlation between FGGY and TP53 expression was analyzed using (A) Gene Expression Omnibus (accession number: GSE39582) and (B) The Cancer Genome Atlas databases. (C) Protein levels of p53, p21 and PCNA in HCT116 cells after FGGY knockdown were assessed by western blotting. GAPDH was used as a loading control. Band intensities were semi-quantified using ImageLab software. *P<0.05 vs. sh-Ctrl. (D) Expression levels of p21 and p53 proteins in HCT116/p53$^{+/+}$ and HCT116/p53$^{-/-}$ cells transduced with sh-FGGY or sh-Ctrl were assessed by western blotting. GAPDH was used as a loading control. Band intensities were semi-quantified using ImageLab software. (E) Viability of HCT116/p53$^{+/+}$ and HCT116/p53$^{-/-}$ cells transduced with sh-FGGY or sh-Ctrl. Results were normalized to viability on day 1. (F) Senescence-associated β-gal staining in HCT116/p53$^{+/+}$ and HCT116/p53$^{-/-}$ cells after FGGY knockdown. Representative images were taken at a magnification of x200. Immunofluorescence images showing co-localization of FGGY in chromatin foci with the SAHF markers (G) H3k9me3 and (H) HP1γ in HCT116/p53$^{+/+}$ and HCT116/p53$^{-/-}$ cells after FGGY knockdown. Representative images were taken at a magnification of x400. *P<0.05 vs. sh-Ctrl HCT116/p53$^{+/+}$ cells. β-gal, β-galactosidase; Ctrl, control; FGGY, FGGY carbohydrate kinase domain containing; H3k9me3, trimethylation of H3K9; sh, short hairpin.

neoplasms (ESCA, STAD and LIHC), whereas its distinctive expression pattern was only observed in CRC, suggesting its potential role as a CRC-specific biomarker for early diagnosis and prognostic evaluation. However, further validation using

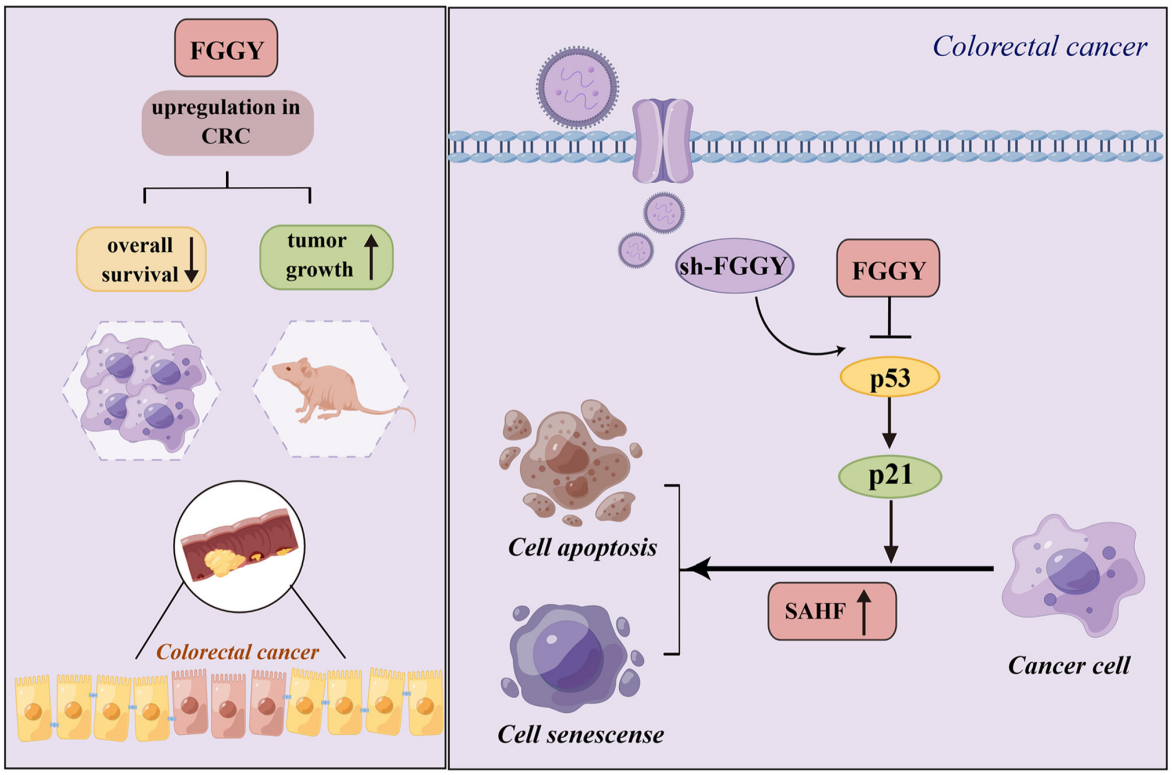


Figure 7. Knockdown of FGGY inhibits cell senescence through the p53/p21 signaling pathway in colorectal cancer. The figure was created using Figdraw (https://www.figdraw.com/). FGGY, FGGY carbohydrate kinase domain containing; sh, short hairpin.

a TMA analysis with a larger number of CRC samples is needed.

The evasion of apoptosis and uncontrolled cell proliferation are well-recognized hallmarks of cancer, which contribute to the disruption of cell homeostasis and an increase in cell number, which are fundamental to tumor development (32,33). L1-FGGY had been shown to be associated with increased cell proliferation and metabolic dysregulation in LUSC (11). The present findings revealed that knockdown of FGGY attenuated tumor growth *in vivo*, and enhanced the apoptosis and inhibited the viability of CRC cells *in vitro*. Given that cell cycle dysregulation may contribute to the promotion of cell proliferation (34), the present study further investigated the impact of FGGY knockdown on cell cycle progression and indicated that knockdown of FGGY induced cell cycle arrest at the $G_0/G_1$ phase in CRC cells. These results suggested that the inhibitory effect of FGGY knockdown on CRC tumor growth may be mediated through inhibiting cell proliferation and inducing cell apoptosis. However, to better understand the role of FGGY in CRC, the effect of FGGY overexpression on cell cycle arrest, apoptosis and colony formation needs to be investigated.

The prospect of FGGY serving as a therapeutic target encouraged an in-depth exploration of its potential mechanism on the growth of CRC cells. Proteomics analysis utilizing iTRAQ identified 236 upregulated and 573 downregulated proteins in CRC cells after FGGY knockdown, whereas the phosphoproteomics analysis identified 145 upregulated and 159 downregulated phosphopeptides. These changes coincided with the modulation of several enriched signaling pathways critical to CRC, including the p53 pathway, SAHF and cellular senescence. These pathways are known to serve essential roles in the development of CRC, thus further implying the potential impact of targeting FGGY in CRC treatment strategies (35,36).

Cellular senescence is a life-threatening process, characterized by a progressive decline in cell proliferation, differentiation and physiological function, thereby resulting in irreversible cell cycle arrest (37). Furthermore, a disruption in this process can result in increased proliferation and progression of tumor cells (34). In light of this, the present study investigated the effects of FGGY on cellular senescence. It was revealed that knockdown of FGGY in CRC cells increased SA-β-gal activity, and the level of SAHF markers HP1γ and H3k9me3 in the nucleus. These findings further implied the essential role of FGGY in regulating cellular senescence and suggested that it may be a promising new target for anticancer therapy.

The p53 protein, known for its tumor-suppressing properties, serves a crucial role in inhibiting cellular proliferation by promoting cell cycle arrest and programmed cell death (38). The p53 pathway is a classical pathway regulating cell senescence (39). As a significantly enriched pathway in the present study, it may be one of potential underlying mechanisms by which FGGY mediates cellular senescence. Thus, restoring p53 function could be considered an effective approach to treat CRC (34,40).

Consistent with this notion, the current study demonstrated that FGGY knockdown resulted in an upregulation of p53 and p21 proteins, while it concurrently led to a downregulation of PCNA expression. These findings contributed insight into the regulatory effects of FGGY on p53, and indicated that p53 knockout abolished the suppressive effect of FGGY

knockdown on the viability of HCT116 cells. It may thus be suggested that inhibition of tumor growth and induction of cell senescence by FGGY knockdown partly depends on p53 activation. In the present study, the very weak negative correlation between FGGY and TP53 was determined using the Pearson correlation coefficient by analyzing the gene expression data from the GEO (GSE39582) and TCGA databases. While these findings could be validated through colorectal TMA analysis, the present study did not assess the protein expression of TP53 and FGGY in TMAs nor analyze their correlation at the protein level in this study. This limitation will be addressed in future research. Additionally, the precise mechanism by which FGGY knockdown activates the p53 pathway require further investigation, including the detection of p53/21 levels and assessment of cellular senescence in FGGY- overexpressing cells.

In the present study, the IVIS Spectrum live-animal imaging system was employed to assess the effect of FGGY knockdown and overexpression on CRC tumor growth in a xenograft mouse model. Due to logistical constraints, fluorescence images of cells inoculated at different time points (0, 1 and 6 days), which would have facilitated longitudinal studies, were not captured. Despite this limitation, the present results clearly demonstrated that FGGY knockdown can suppress CRC tumor growth *in vivo*.

In conclusion, to the best of our knowledge, the present study is the first to reveal that FGGY is abnormally upregulated in CRC tissues, is associated with a poor prognosis and serves an essential role in tumor growth. Notably, the effects of FGGY on inducing cell senescence by partly activating the p53/p21 pathway may be one of underlying mechanisms (Fig. 7). Therefore, FGGY may serve as a promising prognostic biomarker and a potential target for chemotherapy in CRC treatment. The present findings propose novel insights into the mechanism of action of FGGY in CRC.

**Acknowledgements**

Not applicable.

**Funding**

This research received funding from the Natural Science Foundation of Fujian Province (grant no. 2022J011002), the National Natural Science Foundation of China (grant nos. 82274148 and 82274188), the China Postdoctoral Science Foundation (grant no. 2023M740637), and the Fujian Provincial Health Science and Technology Program (grant no. 2024GGA083).

**Availability of data and materials**

The proteomics data generated in the present study may be found in the ProteomeXchange Consortium under accession number PXD059574 or at the following URL: http://proteomecentral.proteomexchange.org/cgi/GetDataset?ID=PXD059574 and its mirror repository Integrated Proteome Resources (iProX) under accession number IPX0010788000 or at the following URL: https://www.iprox.cn/page/project.html?id=IPX0010788000). All other data presented in this study are available from the corresponding author upon reasonable request.

**Authors' contributions**

LYL, LL and ALS contributed to the conceptualization and design of the study. LYL provided administrative support and study conception. YQC contributed to study design and data interpretation, in addition to administrative support. . MZW and YC provided study materials or patients, and collected and analyzed clinical data. SJL and XRZ were responsible for conducting the experiments. Data collection and assembly were carried out by QRX and LJC. Data analysis and interpretation were performed by LHW, YF, TJS and AJ. LYL, LL and ALS confirm the authenticity of all the raw data. The manuscript was collaboratively written by all authors, who read and approved the final version of the manuscript.

**Ethics approval and consent to participate**

Ethics approval for the animal experiments was obtained from the Committee of Fujian University of Traditional Chinese Medicine (approval no. FJTCM IACUC 2019052). Ethics approval for the use of TMAs was granted by the Clinical Research Ethics Committee in Outdo Biotech (nos. SHYJS-CP-1810005, SHYJS-CP-1904003 and SHYJS-CP-1901007) The TMAs used in the present study were commercially available products (Shanghai Outdo Biotech Co., Ltd.), and the requirement for additional ethics approval was waived by the institutional ethics committee due to the commercial nature of the samples and absence of personal information.

**Patient consent for publication**

Not applicable.

**Competing interests**

The authors declare that they have no competing interests.

**References**

1. Sung H, Ferlay J, Siegel RL, Laversanne M, Soerjomataram I, Jemal A and Bray F: Cancer statistics 2020: GLOBOCAN estimates of incidence and mortality worldwide for 36 cancers in 185 countries. CA Cancer J Clin 71: 209-249, 2021.
2. Siegel RL, KD, Miller NS, Wagle and Jemal A: Cancer statistics, 2023. CA cancer J Clin 73: 17-48, 2023.
3. Ladabaum U, Dominitz JA, Kahi C and Schoen RE: Strategies for colorectal cancer screening. Gastroenterology 158: 418-432, .2020.
4. Kanth P and Inadomi JM: Screening and prevention of colorectal cancer. BMJ 374: n1855, 2021.
5. Shen A, Chen Y, Liu L, Huang Y, Chen H, Qi F, Lin J, Shen Z, Wu X, Wu M, *et al*: EBF1-mediated upregulation of ribosome assembly factor PNO1 contributes to cancer progression by negatively regulating the p53 signaling pathway. Cancer Res 79: 2257-2270, 2019.
6. Zhang Y, Zagnitko O, Rodionova I, Osterman A and Godzik A: The FGGY carbohydrate kinase family: Insights into the evolution of functional specificities. PLoS Comput Biol 7: e1002318, 2011.
7. Omelchenko MV, Makarova KS, Wolf YI, Rogozin IB and Koonin EV: Non-homologous isofunctional enzymes: A systematic analysis of alternative solutions in enzyme evolution. Biol Direct 5: 31, 2010.

8. Daoud H, Valdmanis PN, Dion PA and Rouleau GA: Analysis of DPP6 and FGGY as candidate genes for amyotrophic lateral sclerosis. Amyotroph Lateral Scler 11: 389-391, 2010.
9. Van Es MA, Van Vught PW, Veldink JH, Andersen PM, Birve A, Lemmens R, Cronin S, Van Der Kooi AJ, De Visser M, Schelhaas HJ, *et al*. Analysis of FGGY as a risk factor for sporadic amyotrophic lateral sclerosis. Amyotroph Lateral Scler 10: 441-447, 2009.
10. Taylor JA, Shioda K, Mitsunaga S, Yawata S, Angle BM, Nagel SC, Vom Saal FS and Shioda T: Prenatal exposure to bisphenol a disrupts naturally occurring bimodal dna methylation at proximal promoter of fggy, an obesity-relevant gene encoding a carbohydrate kinase, in gonadal white adipose tissues of cd-1 mice. Endocrinology 159: 779-794, 2018.
11. Zhang R, Zhang F, Sun Z, Liu P, Zhang X, Ye Y, Cai B, Walsh MJ, Ren X, Hao X, *et al*: LINE-1 retrotransposition promotes the development and progression of lung squamous cell carcinoma by disrupting the tumor-suppressor gene fggy. Cancer Res 79: 4453-4465, 2019.
12. Sun Z, Zhang R, Zhang X, Sun Y, Liu P, Francoeur N, Han L, Lam WY, Yi Z, Sebra R, *et al*: LINE-1 promotes tumorigenicity and exacerbates tumor progression via stimulating metabolism reprogramming in non-small cell lung cancer. Mol Cancer 21: 147, 2022.
13. Skrzypczak M, Goryca K, Rubel T, Paziewska A, Mikula M, Jarosz D, Pachlewski J, Oledzki J and Ostrowski J: Modeling oncogenic signaling in colon tumors by multidirectional analyses of microarray data directed for maximization of analytical reliability. PLoS One 5: e13091, 2010.
14. Tomczak K, Czerwińska P and Wiznerowicz M: The cancer genome atlas (TCGA): An immeasurable source of knowledge. Contemp Oncol (Pozn) 19: A68-A77, 2015.
15. Marisa L, de Reyniès A, Duval A, Selves J, Gaub MP, Vescovo L, Etienne-Grimaldi MC, Schiappa R, Guenot D, Ayadi M, *et al*: Gene expression classification of colon cancer into molecular subtypes: Characterization, validation, and prognostic value. PLoS Med 10: e1001453, 2013.
16. Li C, Tang Z, Zhang W, Ye Z and Liu F: GEPIA2021: integrating multiple deconvolution-based analysis into GEPIA. Nucleic Acids Res 49: W242-W246, 2021.
17. Rao X, Huang X, Zhou Z and Lin X: An improvement of the 2^(-delta delta CT) method for quantitative real-time polymerase chain reaction data analysis. Biostat Bioinforma Biomath 3: 71-85, 2013.
18. Shen A, Liu L, Chen H, Qi F, Huang Y, Lin J, Sferra TJ, Sankararaman S, Wei L, Chu J, *et al*: Cell division cycle associated 5 promotes colorectal cancer progression by activating the ERK signaling pathway. Oncogenesis 8: 19, 2019.
19. Hubrecht RC and Carter E: The 3Rs and humane experimental technique: Implementing change. Animals (Basel) 9: 754, 2019.
20. Calderón-González KG, Valero Rustarazo ML, Labra-Barrios ML, Bazán-Méndez CI, Tavera-Tapia A, Herrera-Aguirre ME, Sánchez del Pino MM, Gallegos-Pérez JL, González-Márquez H, Hernández-Hernández JM, *et al*: Determination of the protein expression profiles of breast cancer cell lines by quantitative proteomics using iTRAQ labelling and tandem mass spectrometry. J Proteomics 124: 50-78, 2015.
21. Ma YT, Xiao Q, Xu X, Shao and Wang H: iTRAQ-based quantitative analysis of cancer-derived secretory proteome reveals TPM2 as a potential diagnostic biomarker of colorectal cancer. Front Med 10: 278-285, 2016.
22. Kanehisa M and Goto S: KEGG: Kyoto encyclopedia of genes and genomes. Nucleic Acids Res 28: 27-30, 2000.
23. Milacic M, Beavers D, Conley P, Gong C, Gillespie M, Griss J, Haw R, Jassal B, Matthews L, May B, *et al*: The reactome pathway knowledgebase 2024. Nucleic Acids Res 52.D672-D678, 2024.
24. Mi H and Thomas P: PANTHER pathway: An ontology-based pathway database coupled with data analysis tools. Methods Mol Biol 563: 123-140, 2009.
25. Li F, Zhao D, Yang S, Wang J, Li Q, Jin X and Wang W: ITRAQ-based proteomics analysis of triptolide on human A549 lung adenocarcinoma cells.Cell Physiol Biochem 45: 917-934, 2018.
26. Kanehisa M, Furumichi M, Tanabe M, Sato Y and Morishima K: KEGG: New perspectives on genomes, pathways, diseases and drugs. Nucleic Acids Res 45: D353-D361, 2017.
27. Kulak NA, Pichler G, Paron I, Nagaraj N and Mann M: Minimal, encapsulated proteomic-sample processing applied to copy-number estimation in eukaryotic cells. Nat Methods 11: 319-324, 2014.
28. Humphrey SJ, Azimifar SB and Mann M: High-throughput phosphoproteomics reveals in vivo insulin signaling dynamics. Nat Biotechnol 33: 990-995, 2015.
29. Collado M, Blasco MA and Serrano M: Cellular senescence in cancer and aging. Cell 130: 223-233, 2007.
30. Kurz DJ, Decary S, Hong Y and Erusalimsky JD: Senescence-associated (beta)-galactosidase reflects an increase in lysosomal mass during replicative ageing of human endothelial cells. J Cell Sci 113: 3613-3622, 2000.
31. Bannister AJ, Zegerman P, Partridge JF, Miska EA, Thomas JO, Allshire RC and Kouzarides T: Selective recognition of methylated lysine 9 on histone H3 by the HP1 chromo domain. Nature 410: 120-124, 2001.
32. Hanahan D and Weinberg RA: Hallmarks of cancer: The next generation. Cell 144: 646-674, 2011.
33. Hanahan D and Weinberg RA: The hallmarks of cancer. Cell 100: 57-70, 2000.
34. Kramer HB, Lai CF, Patel H, Periyasamy M, Lin ML, Feller SM, Fuller-Pace FV, Meek DW, Ali S and Buluwela L: LRH-1 drives colon cancer cell growth by repressing the expression of the CDKN1A gene in a p53-dependent manner. Nucleic Acids Res 44: 582-594, 2016.
35. Wang G, Fu Y, Hu F, Lan J, Xu F, Yang X, Luo X, Wang J and Hu J: Loss of BRG1 induces CRC cell senescence by regulating p53/p21 pathway. Cell Death Dis 8: e2607, 2017.
36. Shen A, Wu M, Liu L, Chen Y, Chen X, Zhuang M, Xie Q, Cheng Y, Li J, Shen Z, *et al*: Targeting NUFIP1 suppresses growth and induces senescence of colorectal cancer cells. Front Oncol 11: 681425, 2021.
37. Ohtani N, Mann DJ and Hara E: Cellular senescence: Its role in tumor suppression and aging. Cancer Sci 100: 792-797, 2009.
38. Shen Y and White V: p53-dependent apoptosis pathways. Adv Cancer Res 82: 55-84, 2001.
39. Stein GH, Drullinger LF, Soulard A and Dulić V: Differential roles for cyclin-dependent kinase inhibitors p21 and p16 in the mechanisms of senescence and differentiation in human fibroblasts. Mol Cell Biol 19: 2109-2117, 1999.
40. Li XL, Zhou J, Chen ZR and Chng WJ: P53 mutations in colorectal cancer-molecular pathogenesis and pharmacological reactivation. World J Gastroenterol 21: 84-93, 2015.